

An Integration of Rock Physics, AVO Modeling and Analysis for Reservoir Fluid and Lithology Discrimination in A Niger Delta Deep Water Block

D.O. Ogagarue¹ and L.A. Anine²

^{1,2}(Department of Earth Sciences, Federal University of Petroleum Resources, P.M.B. 1221, Effurun, Nigeria).

Abstract: Rock physics and AVO reflectivity and impedance techniques were carried out in an integrated approach to delineate and characterize lithology and fluid effects, as well as map the seismic signature in a soft sandstone reservoir in a deep water block located 25 km offshore, and belonging to the Biafra member of the Agbada formation in the eastern part of the Niger Delta Basin. The study is part of an effort to support seismic data interpretation and ultimately reduce exploration risks associated with deepwater environments. The reservoir sand was qualitatively interpreted to be composed of gas and water, on the basis of its GR, resistivity and density-neutron signatures. Two fluid scenarios were studied comprising different gas saturations (5%, 25%, 50%, 75%, 100%) and a complete water flood. Fluid replacement modeling comprising end member cases of complete brine saturation, 100% gas and 100% oil saturation were also studied for comparison. The Castagna's mud rock line relationship was used to derive the in-situ shear wave log while the linearized Zeoppritz equations were used to model the seismic response at the top of the reservoir by the introduction of the various fluids using the Gassmann's equations. The modeling results indicate that the sandstone reservoir exhibits a Class IV amplitude anomaly, and the Gassmann's simulated reservoir fluids could be clearly delineated within the reservoir except for the in-situ case using log data alone. This result further underscores the application of the Gassmann's fluid replacement modeling in reservoir seismic amplitude studies. Investigation of the AVO characteristics of the true relative amplitude preserved 3D pre-stack time migration full offset (220 m – 6,320 m) field CDP seismic gathers obtained from the block also highlighted the same Class IV AVO anomaly with similar characteristics, suggesting that this is the signature of gas sands in the deep reservoirs of the offshore block studied. The rock physics relations $\lambda - \mu - \rho$, Poisson's Ratio and P-Impedance were most effective in discriminating the gas sands. Their cross-plots generated clusters of points well separated from the background trend. The reservoir is soft sand, and the negative AVO anomaly generated at its top could have been due to a decrease in V_p/V_s Ratio and Poisson's Ratio in relation to the overlying hard-shale layer. The result also revealed amplitude anomalies away from the well bore, identifying possible zones of prospective exploration interests.

Keywords: Attribute analysis, AVO anomaly, fluid replacement modeling, pre-condition, seismic response.

I. Introduction

The amplitudes recorded on a seismic trace are due to contrasts in the elastic properties of rock materials at the boundary separating two half-spaces. The elastic properties basically include compressional and shear wave velocities and density. The elastic properties in turn, are affected by the physical parameters of the rock, such as lithology, porosity, pore fluid and pressure [1].

Amplitude variation with offset (AVO) is a prominent seismic attribute which is widely employed in hydrocarbon detection, lithology identification and reservoir fluid identification, as a result of the fact that seismic amplitudes at the boundaries are affected by variations of the rock physical properties just above and below the boundaries [2]. A compressional seismic energy incident obliquely at an interface generates P- and S-waves which are both reflected and transmitted at the interface. [3] and [4], utilizing the concepts of conservation of stress and displacement across an interface, derived the amplitudes of the reflected and transmitted waves at the layer boundary. The Knott-Zeoppritz equations satisfying four boundary conditions for the reflected and transmitted P- and S-waves in are the following forms [5].

$$A_1 \cos \theta_1 - B_1 \sin \phi_1 + A_2 \cos \theta_2 + B_2 \sin \phi_2 = A_0 \cos \theta_1 \quad 1$$

$$A_1 \sin \theta_1 + B_1 \cos \phi_1 - A_2 \sin \theta_2 + B_2 \cos \phi_2 = A_0 \sin \theta_1 \quad 2$$

$$A_1 Z_1 \cos 2\phi_1 - B_1 \omega_1 \sin 2\phi_1 - A_2 Z_2 \cos 2\phi_1 - B_2 \omega_2 \sin \phi_2 = -A_0 Z_1 \cos 2\phi_1 \quad 3$$

$$A_1 \gamma_1 \omega_1 \sin 2\theta_1 + B_1 \omega_1 \cos 2\phi_1 + A_2 \gamma_2 \omega_2 \sin \theta_2 - B_2 \omega_2 \cos 2\phi_1 = A_0 \gamma_1 \omega_1 \sin 2\theta_1 \quad 4$$

where,

$$Z_i = \rho_i V_{pi}, \omega_i = \rho_i V_{si} \text{ and } \gamma_i = \frac{\omega_i}{Z_i} = \frac{V_{si}}{V_{pi}} \quad i=1, 2, \dots, n$$

The variation of the reflection coefficients with angle or offset forms the basis of AVO analysis.

The Knott-Zeppritz equations are notoriously complex [1], and visualizing how seismic amplitudes are affected by the individual rock physical properties is very difficult [6]. A number of researchers [7], [8], [9], [10], [11], [12] have given simplifications and approximations to the Knott-Zeppritz equations to be able to apply them [13]. The Aki and Richards approximation is appealing because it is parameterized in terms of changes in three terms across an interface; the first involving P-wave velocity, the second involving S-wave velocity and the third involving the density velocity. In matrix form, the Aki-Richards equation is written as:

$$\begin{pmatrix} \sin \theta_1 & \cos \phi_1 & -\sin \theta_2 & \cos \phi_2 \\ -\cos \theta_1 & \sin \phi_1 & -\cos \theta_2 & -\sin \phi_2 \\ \sin 2\theta_1 & \frac{\alpha_1 \cos 2\phi_1}{\beta_1} & -\frac{\rho_2 \beta_2^2 \alpha_1}{\rho_1 \beta_1^2 \alpha_2} \sin 2\theta_2 & \frac{\rho_2 \beta_2 \alpha_1}{\rho_1 \beta_1^2} \cos 2\phi_2 \\ \cos 2\phi_1 & -\frac{\beta_1}{\alpha_1} \sin 2\phi_1 & -\frac{\rho_2 \alpha_2}{\rho_1 \alpha_1} \cos 2\phi_2 & -\frac{\rho_2 \beta_2}{\rho_1 \alpha_1} \sin 2\phi_2 \end{pmatrix} \begin{pmatrix} R_p \\ R_s \\ T_p \\ T_s \end{pmatrix} = \begin{pmatrix} -\sin \theta_1 \\ -\cos \theta_1 \\ \sin 2\theta_1 \\ -\cos 2\phi_1 \end{pmatrix} \quad 5$$

The three-term Aki-Richards equation is given by:

$$R_p(\theta) = a \frac{\Delta V_p}{V_p} + b \frac{\Delta V_s}{V_s} + c \frac{\Delta \rho}{\rho}, \quad 6$$

where,

$$a = \frac{1}{(2\cos^2 \theta)}, \quad b = -\left[4 \frac{V_s^2}{V_p^2} \right] \sin^2 \theta, \quad c = 0.5 - \left[\left(2 \frac{V_s^2}{V_p^2} \right) \sin^2 \theta \right], \text{ with:}$$

$$V_p = \frac{V_{p1} + V_{p2}}{2}, \quad \Delta V_p = V_{p2} - V_{p1}$$

$$V_s = \frac{V_{s1} + V_{s2}}{2}, \quad \Delta V_s = V_{s2} - V_{s1}$$

$$\rho = \frac{\rho_1 + \rho_2}{2}, \quad \Delta \rho = \rho_2 - \rho_1$$

$$\theta = \frac{\theta_1 + \theta_2}{2}, \text{ where } \theta_t = \sin^{-1} \left[\frac{V_{p2}}{V_{p1}} \sin \theta_i \right]$$

V_p , V_s and ρ are average compressional and shear velocity, and density across the interface; ΔV_p , ΔV_s and $\Delta \rho$ are average change in compressional and shear wave velocity, and density across the interface and $R(\theta)_p$ is the reflection coefficient as a function of angle of incidence.

[14] algebraically reformulated the equation, separating it into three reflection terms (Equ. 7), each weaker than the previous term.

$$R_p(\theta) = A + B \sin^2 \theta + C \tan^2 \theta \sin^2 \theta \quad 7$$

where

$$A = \frac{1}{2} \left[\frac{\Delta V_p}{V_p} + \frac{\Delta \rho}{\rho} \right] \quad \text{is the intercept}$$

$$B = \frac{1}{2} \frac{\Delta V_p}{V_p} - 4 \left[\frac{V_s}{V_p} \right]^2 \frac{\Delta V_s}{V_s} - 2 \left[\frac{V_s}{V_p} \right]^2 \frac{\Delta \rho}{\rho} \quad \text{is the gradient}$$

$$C = \frac{1}{2} \frac{\Delta V_p}{V_p} \quad \text{is the curvature, which is significant for incident angles } > 30^\circ.$$

The [14] approximation is the AVO equation utilized for this study.

The use of AVO analysis in hydrocarbon exploration started with the work of [15]. Since then, several techniques have been used to obtain AVO signature, including conventional AVO attribute study, together with more recent techniques such as spectral analysis and a modeling-based approach as tools for fluid and lithology discrimination in clastic environments [13], [16], [17], [18], [19], [20], [21], [22], [23], [24]. All of these works are aimed at gaining insight and understanding of the reservoir fluid and lithology to aid interpretation and reduce exploration risks.

[16] classified three classes of AVO anomalies for gas sands encased in shales, namely Class I, II and III. Their classification was based only on the P-wave normal incidence reflection coefficient (intercept A). Class I sands are high impedance sands relative to the overlying shales; they have positive AVO intercept and reflection coefficient values decrease (i.e. become less positive, implying decrease) with offset, giving a negative AVO gradient. Class II sands have small impedance contrast; the AVO intercept is near zero, but may be positive or negative. Reflection coefficient values may become less positive or more negative with offset, giving negative AVO gradient. The reflection amplitudes may therefore increase or decrease with offset. Class III sands have lower impedance relative to the overlying shale; AVO intercept is negative, and reflection coefficient values become more negative (implying increase) with offset, giving negative AVO gradient. Using a combination of the intercept and gradient, [25] defined a Class IV sands for the case where initially negative reflection coefficients become less negative (implying decrease) with increasing offset, giving negative intercept and positive gradient.

In this research, we used a combination of rock physics, AVO modeling and analysis with the objective of deriving effective AVO attributes to delineate and characterize a sandstone reservoir in a deep water block in the eastern part of the Niger Delta in terms of its fluid and lithology. [26] describes a method employing basic rock physics, AVO and seismic amplitude inversion to discriminate fluid using pre-stack seismic data. From the reviewed literatures, rock physics templates and AVO attributes relevant to the data provided were identified in an attempt to optimize time and reduce computational complexities on application to the data. The study is part of an effort to support seismic data interpretation and reduce exploration risks associated with the block, and to identify exploration development opportunities away from the well location.

Location and Geology

The study area is located in a deep water offshore block, south-eastern part of the Niger Delta (Fig. 1). The Niger Delta is a prolific hydrocarbon province with a regressive succession of clastic sediments which reaches a maximum thickness of 10-12 km. The province contains only one identified petroleum system, known as the Tertiary Niger Delta [27], [28], [29], [30], [31]. The delta is divided into an upper series of massive sands and gravels (Benin Formation), deposited under continental conditions. This grades downward into interbedded shallow marine and fluvial sands, silts and clays, which form the paralic sequence of the Agbada Formation. The Agbada Formation grades into the massive and monotonous marine shales. Most of the hydrocarbons are in the sandstones of the Agbada Formation, where they are trapped in rollover anticlines fronting growth faults in channels and barrier sandstone bodies. Offshore deep-water Nigeria is entering its third decade of exploitation [32]. The sediments in the study area are deposited in the deltaic and prodeltaic environments, with the reservoirs mainly dominated by interplay of lower and upper shoreface facies, distributary channel facies and tidal deposits.

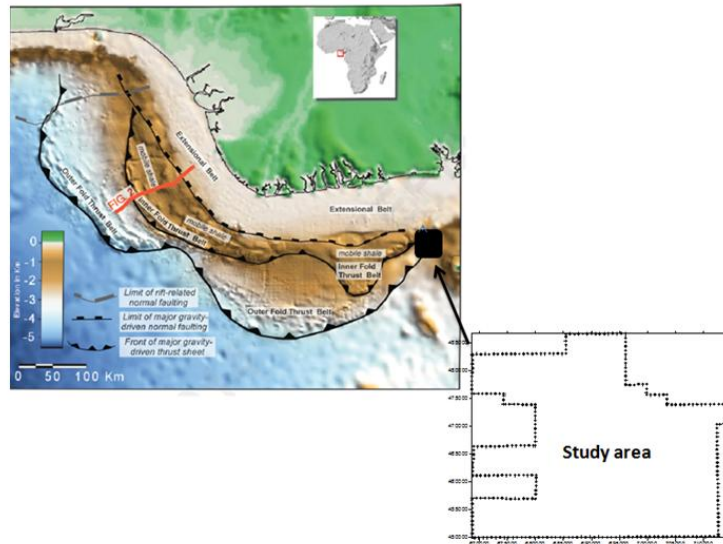


Figure 1: Map of the Niger Delta showing the study area. Major structural features of the delta are labeled shown over a bathymetric map from [33] (modified from [32]).

II. Materials and Methods

Data used for this study comprise a suite of well logs containing GR, resistivity, sonic, density and neutron logs, and a 60-fold pre stack time migrated CDP gathers with offset range of 220 m to 6,320 m. The reservoir was identified on the basis of its relatively low GR values and high resistivity. The caliper log indicates that there is no washout in the reservoir. The in-situ reservoir fluid, identified on the basis of the density-neutron plots is made up of a homogeneous mixture of gas and water. The gas-saturated portion of the reservoir was identified by its wide neutron-density cross-over, plotted using a sandstone compatible scale. Fig.2 shows the well data and seismic gathers used for the study.

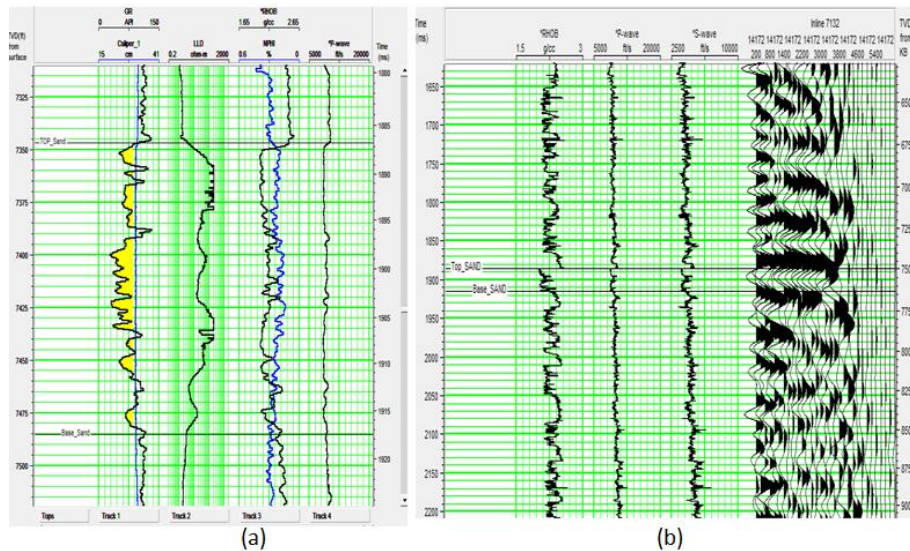


Figure 2: Section through the well showing the reservoir studied. (a) Well log data showing GR, LLD, RHOB-NPHI, P-wave logs and reservoir top and base. (b) Section showing RHOB, P-wave and Castagna-derived S-wave velocity logs, and full offset CDP PSTM gathers at the well location.

In the first instance, we carried out frequency analysis of the seismic gathers at the well location to have an understanding of the useful frequency range present in the data (Fig. 3).

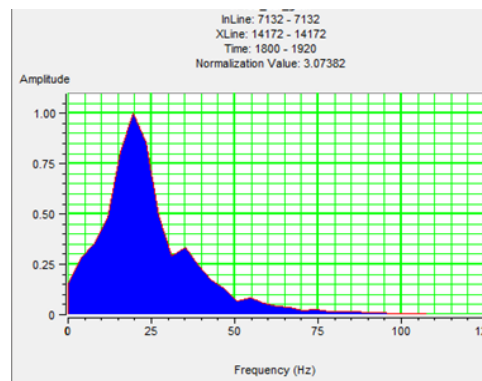


Figure 3: Frequency analysis of seismic gathers at the well location. Maximum frequency of 45 Hz was chosen to be adequate for deriving zero phase wavelet for generation of synthetics.

Thereafter, we performed a well-to-seismic tie to obtain a correction for the P-wave log at the well location. To achieve this, we used a statistical least squares approach to estimate an initial zero-phase wavelet of length 180 ms from the seismic data alone, using a maximum frequency of 45 Hz based on Fig. 3. Eleven CDP gathers, five CDPs on both sides of the well were used for the wavelet estimation. Following from this, a five-trace synthetic seismogram was generated by convolution of the wavelet and earth reflectivity function at the well location. These were correlated to composite traces computed from the neighboring traces at the well location to obtain a good match between the well and seismic data. A combination of the well and seismic data were finally used to obtain a better wavelet which we used to refine the correlation to obtain good match between the seismic and well data. A corrected sonic P-wave log was then obtained which was used for the rock physics and AVO modeling and analysis.

Next, we empirically generated an S-wave log from the corrected P-wave sonic log using the Castagna's mud rock line relationship and created in-situ synthetic seismic traces using the [14] modification of the Aki-Richards linearized Zeoppritz equations. Thereafter, we used the standard Biot-Gassmann's equations implemented in the Hampson-Russell AVO software to perform fluid replacement modeling. In an initial iteration, hydrocarbon effects in the compressional, shear and density logs were backed out to represent a truly brine-bearing case as input to the fluid substitution. Subsequent iterations were performed, whereby gas was introduced into the reservoir in the order of 5%, 25%, 50%, 75% and 100% respectively. In each fluid replacement modeling, we created new elastic and density logs and generated synthetic traces. We also modeled the seismic response for the end member cases of 100% brine, 100% gas and 100% oil for comparison. The objective was to model the seismic response at the interface between the reservoir and overlying thick shale to gain an understanding of the observed variation with offset anomaly resulting from changes in fluid saturation from the in-situ case to the different pore fluid scenarios calculated by the Gassmann's fluid substitution. In all the cases, the modeling was carried out at well depths 3,550 ft to 10,400 ft but detailed ray-tracing was done at the target reservoir depth of 7,502 ft to 7,640 ft (138 ft reservoir interval). Using rock physics relationships, we generated crossplots to aid in the litho-fluid discrimination using log data alone.

Lastly, AVO analysis was performed on the CDP gathers. Prior to this, we pre-conditioned the gathers by generating CDP super gathers and applying trim statics, and thereafter converted them from offset to incident angles. The AVO analysis was performed on the angle gathers.

III. Results and Discussion

Fluid replacement modeling from the in-situ fluid to the wet case (100% water) caused a reduction in both P-wave velocity and density. Fig. 4 shows the result of fluid replacement modeling from the wet case in the reservoir. The compressional wave velocity and density respectively increased and decreased, with the introduction of gas into the reservoir, the percentage increase and decrease reducing with increase in gas saturation. Principally it can be observed on the compressional sonic and density logs that the gas separation is large enough to make gas visible on the seismic, even at small accumulation in the reservoir. Whereas bulk density decreased slightly with oil substitution, the compressional velocity was largely unchanged with oil replacing brine. S-wave velocity marginally increased with gas or oil replacing the in-situ fluid. Fig. 5 shows the end member fluid substitution cases of 100% gas and 100% oil substitution in comparison to the in-situ case.

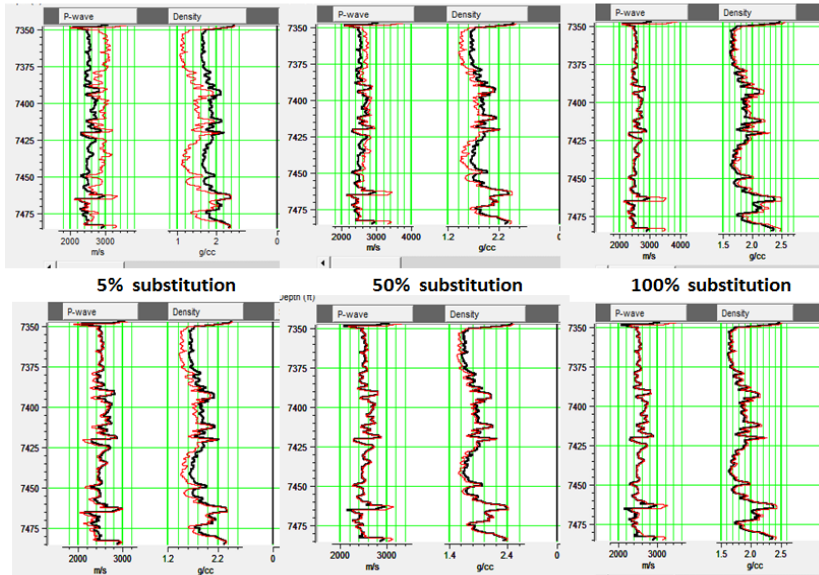


Figure 4: Gassmann fluid replacement modeling: Top: Gas substitution; Bottom: Oil substitution. The black curve is the wet case and the red is the Gassmann modified log.

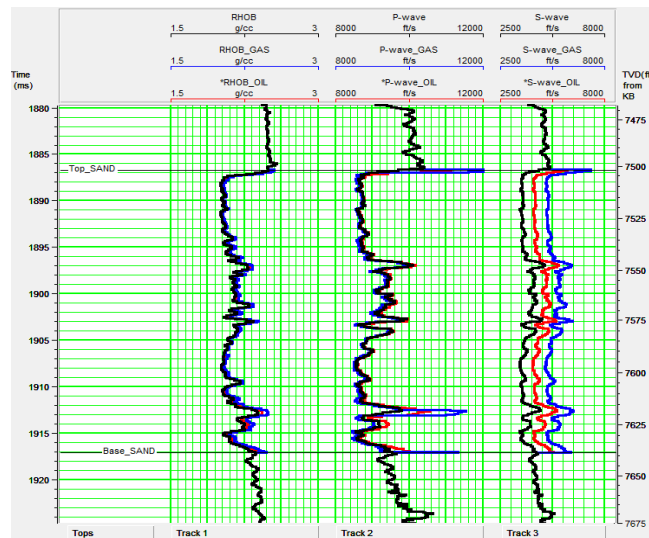


Figure 5: Fluid substitution effects on end member cases: Track 1: Bulk density Track 2: P-wave velocity Track 3: S-wave velocity (Insitu = Black; 100%Gas = Blue; 100%Oil = Red)

Fig. 6 shows AVO attribute logs created from the fluid replacement modeling for the end-member cases. Both V_p/V_s Ratio and Poisson's Ratio decreased across the reservoir substituting to gas or oil from the in-situ case. The same trend was observed in modeling oil or gas from a fully water saturated case. V_p/V_s Ratio and the Poisson's Ratio are lowest in the gas saturation scenario. The marginal decrease in these AVO attributes indicate that hydrocarbon effects should be well expressed at seismic scale in the offset domain. Low V_p/V_s and Poisson's Ratio in gas saturated conditions may be due to increase in pore pressure [34]. The average effective porosity across the reservoir is 32.6%. Increased pore pressure tends to make gas less compressible, resulting in increase in compressional velocity. This probably explains the increase in compressional velocity upon gas substitution in the deep reservoir from the wet case.

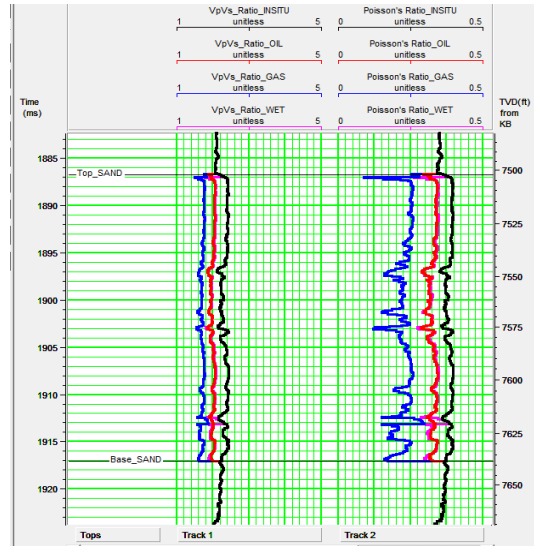


Figure 6: Vp/Vs_Ratio and Poisson's_ratio across the reservoir. Track 1: Vp/Vs_Ratio; Track 2: Poisson's_Ratio (Black = Insitu case; Red = 100% oil; Blue = 100% gas).

Fig. 7 shows the AVO response from the changes in elastic parameters resulting from the different fluid substitution scenarios picked from the top of the reservoir at the shale-sandstone boundary. All of the AVO responses, including the in-situ case, showed decrease in amplitude with offset, having negative reflection coefficients which became less negative with increasing offset. The results do not belong to any of the three AVO classifications given by [16], based on intercept only, but agree with the [25] augmented Rutherford and Williams' classification based on both intercept and gradient. The results show Class IV anomaly, having negative intercept and positive gradient. The AVO intercept is lowest for the wet case (-1.08). The value increased, becoming more negative with increase in gas substitution. The AVO intercept was -1.15 at 100% gas saturation. Class IV sands have been shown to occur when a porous sand is overlain by high-velocity unit, such as hard shale, siltstone, tightly cemented sand or carbonate, such as is the case in this study where the reservoir is overlain by a high-velocity shale unit (Fig. 2a).

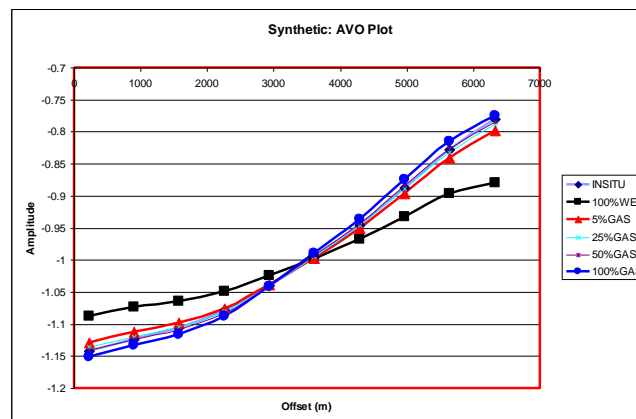


Figure 7: Picked events from the reservoir top on synthetic seismograms.

Fig. 8 shows a concatenated synthetic CDP gather of the in-situ and end-member fluid substitution modeling for the wet, gas and oil cases. AVO analysis performed on this volume did not show any obvious anomaly on the $A*B$ product. However, the scaled Poisson's Ratio change ($aA+bB$) highlighted a fairly strong amplitude anomaly at the target (Fig. 9). The plot shows a strong negative (orange) response at the top of the reservoir, indicating a drop in Poisson's Ratio.

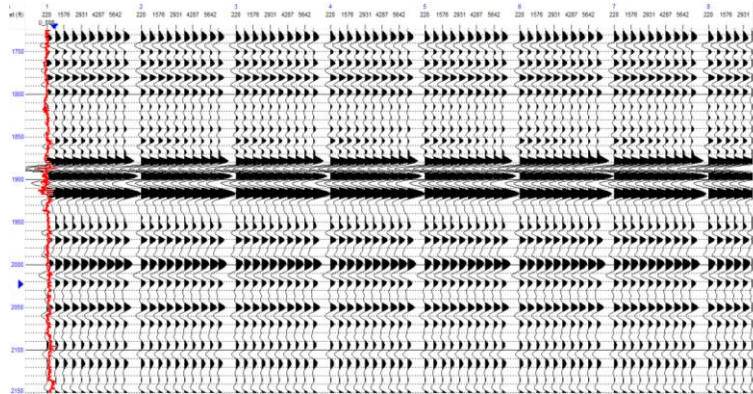


Figure 8: Concatenated synthetic gathers showing amplitude anomaly at the target.

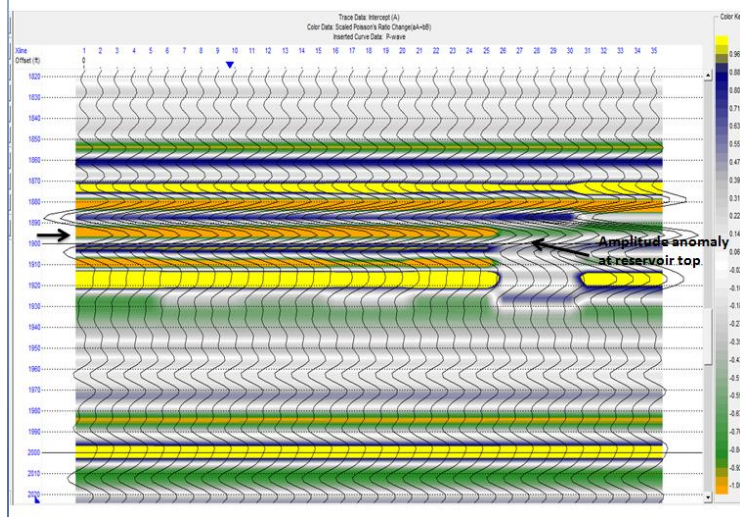


Figure 9: Scaled Poisson's Ratio attribute volume on concatenated synthetic seismogram for the insitu and end-member Gassmann's fluid replacement modeling cases.

To have a general view of how lithology influences the reservoir physical rock properties, several rock physics relationships were cross-plotted for the insitu reservoir fluids and results obtained from 50% gas substitution. One important observation made from the log data cross-plot analysis was that none of the rock physics relationships was able to discriminate the insitu reservoir fluids and lithology (Fig. 10), but a number of the relationships clearly discriminated the fluids and lithology with the Gassmann's fluid substitution results as they clearly show a cluster of points away from the background trend. This underscores the usefulness of the Gassmann fluid substitution in seismic amplitude studies using well log data. For this study, the Mu-Rho versus Lambda-Rho and Poisson's Ratio versus P-Impedance cross-plots have shown the greatest ability to discriminate the reservoir fluids and lithology based on the large separation between the gas sand and background trend. Fig. 11 shows cross-plot analysis for the 50% gas modeling results.

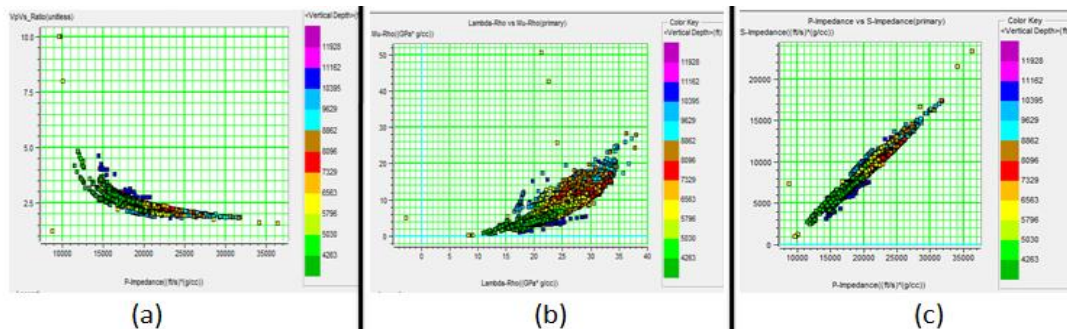


Figure 10: Rock physics relation cross-plot analysis for in-situ well log data: (a) V_p/V_s Ratio versus P-impedance; (b) Mu-Rho versus Lambda-Rho (c) P-Impedance versus S-Impedance.

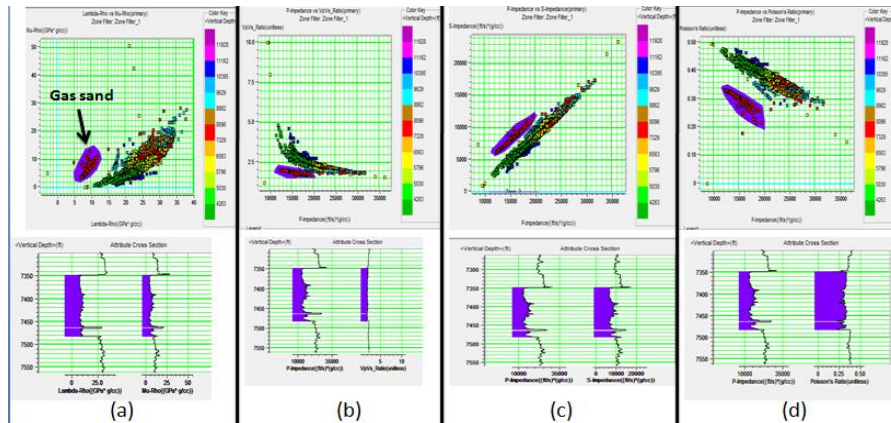


Figure 11: Cross-plot analysis using 50% gas replacement modeling. (a) Mu-Rho versus Lambda-Rho (b) Vp/Vs_Ratio versus P-Impedance (c) P-Impedance versus S-Impedance (d) Poisson's Ratio versus P-Impedance. The attribute cross-section is shown below for each attribute cross-plot. Cross-plot (a) and (d) show the largest cluster separation.

So far, the log based rock physics and AVO modeling have established the presence of a fairly strong AVO anomaly due to variations in gas saturation in the reservoir, whose amplitude decrease with increasing offset, having a negative intercept that became less negative with offset, and a positive gradient. Investigation of the AVO characteristics of the pre-stack field seismic data in the vicinity of the reservoir highlighted the same Class IV AVO anomaly with similar characteristics. Fig. 12 shows the result of AVO gradient analysis performed on the pre-stack gathers. The seismic response and A*B crossplot at the target reservoir highlighted the same Class IV AVO anomaly seen from the log modeling. The A*B Product and Scaled Poisson's Ratio (aA+bB) show the sand top and prospective exploration zones away from the target reservoir.

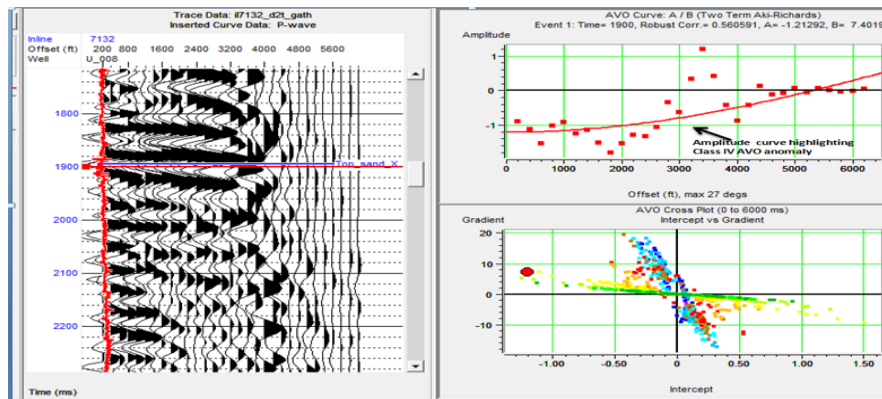


Figure 12 (a): AVO gradient analysis of field seismic data at target, highlighting Class IV AVO anomaly.

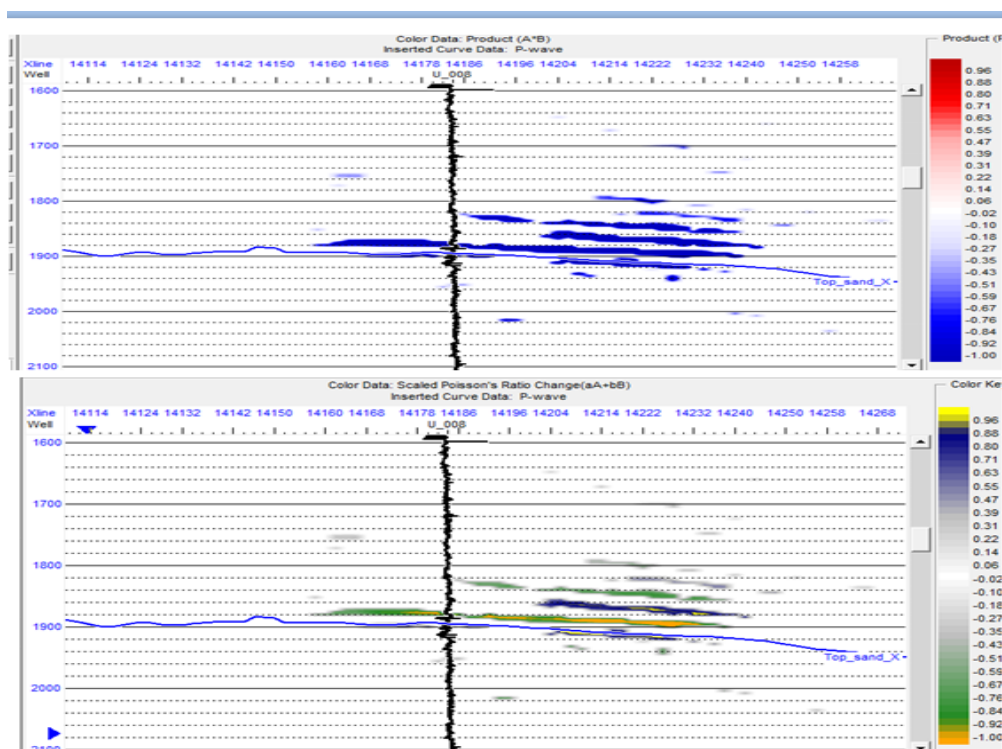


Figure 12 (b): AVO analysis result: top: A*B Product Bottom: Scaled Poisson's Ratio (aA+bB). The plots highlight negative amplitude anomaly at the reservoir top. Other prospective exploration zones can also be identified from the AVO attribute volumes.

IV. Conclusion

Success in prospect evaluation requires the use of all available data to gain insight and reduce exploration risk. Integrating results from rock physics relations, AVO modeling and analysis is critical and of great importance in achieving this objective. Using these techniques, we have detected gas sands in the deep water block offshore Niger Delta. The gas sands generated Class IV AVO anomaly, suggesting that this is the signature of gas sands in the deep reservoirs of the offshore block studied. The study further showed that the rock physics relations, $\lambda - \mu - \rho$, Poisson's Ratio and P-Impedance were most effective in discriminating the gas sands. Their cross-plots generated clusters of points well separated from the background trend. The reservoir is soft sand, and the negative AVO anomaly generated at its top could have been due to a decrease in V_p/V_s Ratio and Poisson's Ratio in relation to the overlying hard-shale layer.

Acknowledgement

The authors are grateful to CGG Geosoft for donating the software used for this study.

References

- [1]. R.H. Tatham, V_p/V_s and lithology, *Geophysics*, 47, 1982, 336-344.
- [2]. H. Zhang and J. Brown, A review of AVO analysis, CREWES Research Report, Vol. 13, 2001.
- [3]. C.G. Knott, Reflexion and refraction of elastic waves with seismological applications, *Phil. Mag.*, 5th ser. 48, 1899, 64-97.
- [4]. K. Zeppritz, Erdbebenwellen, VIII B, On the reflection and propagation of seismic waves: *Gottinger Nachrichten*, 1, 1919, 66-84.
- [5]. R.E. Sheriff and L.P. Geldart, *Exploration Seismology*, Cambridge University Press, Vol. 1, 1982.
- [6]. J.P. Castagna, Petrophysical imaging using AVO, *The Leading Edge*, 12(3), 1993, 172-178.
- [7]. R. Bortfeld, Approximations to the reflection and transmission coefficients of plane longitudinal and transverse wave, *Geophys. Prosp.*, 9, 1961, 485-503.
- [8]. P.G. Richards and C.W. Frasier, Scattering of elastic waves from depth-dependent inhomogeneities, *Geophysics*, 41, 1976: 441-458.
- [9]. K. Aki, and P.G. Richards, *Quantitative seismology: Theory and methods*, W.H. Freeman and Co., 1980.
- [10]. R.T. Shuey, A simplification of the Zeppritz equations, *Geophysics*, 50, 1985, 609-614.
- [11]. G.C. Simth and P.M. Gidlow, Weighted stacking for rock property estimation and detection of gas, *Geophys. Prosp.*, 35, 1987, 993-1014.
- [12]. J.L. Fatti, G.C. Smith, P.C. Vail, P.J. Strauss and P.R. Levitt, Detection of gas in sandstone reservoirs using AVO analysis: A 3D seismic case history using the Geostack technique, *Geophysics*, 59, 1994, 1352-1376.
- [13]. M.T. Oladapo, Linearization of Zeppritz equations and practical utilization, *Int. J.Phys. Sci.*, 8(24), 2013, pp. 1298-1306.
- [14]. R. Wiggins, G.S. Kenny and C.D. McClure, A method for determining and displaying the shear velocity reflectivities of a geological formation. European Patent

- [15]. Application 0113944, 1983.
- [16]. W.J. Ostrander, Plane wave reflection coefficients for gas sands at non-normal angles of incidence, *Geophysics*, 49, 1984, 1637-1648.
- [17]. S.R. Rutherford and R.H. Williams, Amplitude-versus-offset variations in gas sands, *Geophysics*, 54, 1989, 680-688.
- [18]. J.P. Castagna and M.M. Backus, AVO analysis-tutorial and review, in Castagna, J. and Backus, M.M., eds., *Offset-dependent reflectivity – Theory and practice of AVO analysis*; Soc. Expl. Geophys., 1993, 3-37.
- [19]. J.P. Castagna and H.W. Swan, Principles of AVO crossplotting, *The Leading Edge*, 16, 1997, 337-342.
- [20]. B. Goodway, T. Chen and J. Downton, Improved AVO fluid detection and lithology discrimination using Lamé's petrophysical parameters; " $\lambda\rho$ ", " $\mu\rho$ " and " λ/μ " fluid stack from P and S inversions, 67th Ann. Intern. Mtg., Soc. Expl. Geophys., Expanded Abstracts, 1997, 183-186.
- [21]. K. Wapenaar, Amplitude-variation-with-angle behaviour of self-similar interfaces, *Geophysics* 64, 1999, 1928-1938.
- [22]. O. Ujuanbi, J.C. Okolie and S.I. Jegede, Lambda-mu-rho technique as a viable tool for lith-fluid discrimination – The Niger Delta example, *Int. J. Phys. Sci.*, 2(7), 2008, 173-176.
- [23]. A.C. Ekwe, K.M. Onuoha and N. Osayande, Fluid and lithology discrimination using rock physics modeling and Lambdamurho inversion: An example from onshore Niger Delta, Nigeria, adapted from extended abstract prepared in conjunction with oral presentation at AAPG Intern. Conf. Exhib., Milan, Italy, 2012.
- [24]. P.A. Enikanselu, and A. Adekanle, Detection of hydrocarbon reservoirs using AVO technique offshore Niger Delta, *Canadian Journal of Computing in Mathematics, Natural Sciences, Engineering and Medicine*, 3(7), 2012, 261-269.
- [25]. S.A. Ugwu and C.N. Nwankwo, Fluid substitution and AVO modeling for hydrocarbon and lithology discrimination in X-Field, Offshore Niger Delta, *Stand. Sci. Res. Essays*, 2(8), 2014, 333-344.
- [26]. J.P. Castagna, H.W. Swan and D.I. Foster, Framework for AVO gradient and intercept interpretation, *Geophysics*, 63, 1998, 948-956.
- [27]. B.H. Russell, K. Hedlin, F.J. Hilterman and L.R. Lines, Fluid-property discrimination with AVO: A Biot-Gassmann perspective, *Geophysics*, 68, 2003, 29-39.
- [28]. J.M. Orife and A.A. Avbovbo, Stratigraphic and unconformity traps in the Niger Delta: AAPG Bulletin. 66(2): 1982, 251-262.
- [29]. C.M. Ekweozor and E.M. Daukoru, Niger Delta depobelt portion of the Akata-Agbada petroleum system, AAPG Memoir 60, 1994, 599-604.
- [30]. H. Kulke, *Regional Geology of the world, part 2: Africa, America, Australia, Antarctica*: Berlin Gebrüder borntraeger, Kulke Ed.: 1995 143-172.
- [31]. T.J.A. Reijers, S.W. Peter and C.S. Nwajide, The Niger Delta Basin: In Reijers, T.J.A. Ed., *Selected Chapters on Geology*; SPDC, Warri, 1996, 103-118.
- [32]. M.L.W. Tuttle, R.R. Chapentier and M.E. Brownfield, The Niger Delta petroleum system: Niger Delta province, Cameroon and Equatorial Guinea, Africa, 1999: <http://greenwood.cr.usgs.gov/energy/OF99-50H/ChapterA.htm#TOP>
- [33]. C.D. Connors and B.J. Radovich, Multiage plays in offshore Niger Delta: Hidden plays of Neogene shale structures, and robust lower Miocene to paleogene deposition, *Sedimentary Basin: Origin, Depositional Histories and Petroleum System*, GCSSEPM, 2014.
- [34]. F. Corredor, J.H. Shaw and F. Bilotti, Structural styles in deepwater fold and thrust belts of the Niger Delta, AAPG Bulletin, 89, 2005: 753-780.
- [35]. T. Vanorio and G. Mavko, Vp/Vs Ratio in gas-pressured saturated sandstone, SEG Ann. Mtg., 2006, 1545.